Available online at www.sciencedirect.com

ScienceDirect

www.elsevier.com/locate/jes

JES JOURNAL OF ENVIRONMENTAL SCIENCES

www.jesc.ac.cn

Ca^{2+} and OH^- release of ceramsites containing anorthite and gehlenite prepared from waste lime mud

Juan Qin[1], *Chuanmeng Yang*[1], *Chong Cui*[1,*], *Jiantao Huang*[1], *Ahmad Hussain*[1], *Hailong Ma*[2]

1. *School of Materials Science and Engineering, Nanjing University of Science and Technology, Nanjing 210094, China*
2. *Institute of Ethnic Preparatory Education, Ningxia University, Yinchuan 750021, China*

ARTICLE INFO

Article history:
Received 13 October 2015
Revised 29 February 2016
Accepted 7 March 2016
Available online 22 April 2016

Keywords:
Lime mud
Ceramsite
Gehlenite
Calcium ion
PH value

ABSTRACT

Lime mud is a kind of solid waste in the papermaking industry, which has been a source of serious environmental pollution. Ceramsites containing anorthite and gehlenite were prepared from lime mud and fly ash through the solid state reaction method at 1050°C. The objective of this study was to explore the efficiency of Ca^{2+} and OH^- release and assess the phosphorus and copper ion removal performance of the ceramsites via batch experiments, X-ray diffraction (XRD) and scanning electron microscopy (SEM). The results show that Ca^{2+} and OH^- were released from the ceramsites due to the dissolution of anorthite, gehlenite and available lime. It is also concluded that gehlenite had stronger capacity for Ca^{2+} and OH^- release compared with anorthite. The Ca^{2+} release could be fit well by the Avrami kinetic model. Increases of porosity, dosage and temperature were associated with increases in the concentrations of Ca^{2+} and OH^- released. Under different conditions, the ceramsites could maintain aqueous solutions in alkaline conditions (pH = 9.3–10.9) and the release of Ca^{2+} was not affected. The removal rates of phosphorus and copper ions were as high as 96.88% and 96.81%, respectively. The final pH values of both phosphorus and copper ions solutions changed slightly. The reuse of lime mud in the form of ceramsites is an effective strategy.

Introduction

Lime mud is a kind of by-product achieved during the causticization reaction of the alkali recycling process in the paper industry (Cheng et al., 2009). Its major chemical component is calcium carbonate ($CaCO_3$). Due to high alkalinity (pH = 9.7–13.5) and the existence of heavy metal ions (*e.g.*, Cr, Mn and Fe) (Martins et al., 2007; Sthiannopkao and Sreesai, 2009; Zhang et al., 2013), lime mud is classified as toxic industrial waste. It has been estimated that about 0.5 tons of lime mud can be produced per ton of pulp (Wirojanagud et al., 2004). In 2011, the production of lime mud was about 10 million tons in China, and it continues to increase significantly with the growing demand for paper (Sun et al., 2013). Mostly, lime mud is disposed by landfilling, which results in land consumption and environmental pollution (Huber et al., 2014; Liu et al., 2011; Monte et al., 2009). Therefore, there is an urgent need for proper treatment methods for lime mud.

Ceramsites contain oxides like Al_2O_3, SiO_2, Fe_2O_3, FeO, CaO, MgO, Na_2O and K_2O. These components are useful for construction materials, *i.e.*, bricks, fine aggregate in mortars and ceramic materials, and filter media in reactors for treating municipal and industrial wastewater (Xu et al., 2006, 2008).

* *Corresponding author*. E-mail: cuichong@njust.edu.cn (Chong Cui).

http://dx.doi.org/10.1016/j.jes.2016.03.013

Considering the chemical composition of lime mud and fly ash, they have the possibility to be reused as ceramsites (Cernec et al., 2005; Ahmadi and Al-Khaja, 2001).

Lime mud is characterized by high calcium content, so ceramsites prepared from lime mud and fly ash can be considered calcium-rich materials. Previous studies have showed that calcium-rich materials can effectively remove phosphorus from wastewater (Kaasik et al., 2008; Liira et al., 2009; Vohla et al., 2011), because Ca^{2+} and OH^- can be released from calcium-rich materials and react with phosphate to form hydroxyapatite at the optimal pH value (Song et al., 2006; Liu et al., 2003; Yin et al., 2011). In addition, heavy metal ion removal from wastewater is also closely related to pH (Stafiej and Pyrzynska, 2008; Tofighy and Mohammadi, 2011; Li et al., 2011). For example, when the initial pH of an aqueous solution is higher than 6.0, precipitation of Cu(II) ions as $Cu(OH)_2$ will occur spontaneously (Yan et al., 2012). The required pH increase can be achieved in several ways, such as aeration (Battistoni et al., 1998) or addition of NaOH, lime or $Mg(OH)_2$ (Fujimoto et al., 1991). Ceramsites prepared from lime mud and fly ash can release OH^- independently, which will avoid the consumption of other alkaline chemicals. This type of ceramsite will not only alleviate the environmental pollution caused by lime mud but also provide economical and multi-functional materials for wastewater treatment.

The purpose of this study was to assess the efficiency of Ca^{2+} and OH^- release from ceramsites prepared from lime mud and fly ash. On the basis of batch experiments, the influences of formulation, dosage, temperature, initial pH and contact time on the efficiency were investigated. The mechanism of Ca^{2+} and OH^- release was explained and the Ca^{2+} release was represented by the Avrami kinetic model. The ceramsites were also applied in the treatment of wastewater containing phosphorus and copper ions.

1. Experimental

1.1. Preparation of the ceramsites

The ceramsites were prepared from lime mud, fly ash and some additives (diatomite, sawdust, kaolin). Lime mud was collected from the alkali recycling process of Xuzhou paper company, China. Fly ash was obtained from a power plant of Nanjing, China. Sawdust was obtained from a wood processing factory of Nanjing, China. Diatomite and kaolin were purchased from Nanjing Dongji New Building Materials Co., Ltd., China. The chemical compositions of the raw materials were analyzed (BE EN 196-2, 2013) and are shown in Table 1. It can be seen that the lime mud has a calcium oxide content as high as 45.18 wt.%. Its loss on ignition (L.O.I) is 37.16 wt.%, which is associated with the decomposition of $CaCO_3$. Therefore, lime mud was used as a source of calcium oxide and also as a pore-forming material. Fly ash contains a substantial amount of SiO_2 (53.54 wt.%) and Al_2O_3 (28.80 wt.%). When fly ash is used as the raw material for the sintered ceramsites, it can compensate for the disadvantages of lime mud. Lignin is an important component of sawdust.

Table 2 – Proportions of the mixtures for the formulations (wt.%).

Sample No.	Lime mud	Fly ash	Diatomite	Sawdust	Kaolin
LF	40	60	0	0	0
LFD	40	55	5	0	0
LFS	50	45	0	5	0
LFSK	50	40	0	5	5

The raw materials were mixed according to Table 2 in a laboratory mortar mixer (Model JJ-5) for 10 min. Then, the mixture was put into a pelletizing machine (Model YK-80) to form pelletized raw ceramsites with particle sizes of 3–5 mm. In this process, the amount of water necessary for formation of pellets (2–8 wt.%) was added to the mixture. Later, the raw ceramsites were dried in air at room temperature for 2 days and then kept in an oven at 105°C for 24 hr. After that, the raw ceramsites were sintered in a laboratory-type electrical sintering furnace (Model HTF1400). The heating rate was 10°C/min below 800°C and 5°C/min above 800°C. Samples were soaked at 800°C for 1 hr and at 1050°C for 2 hr. Finally, the furnace was left to cool for all ceramsites.

1.2. Batch experiments

Batch experiments to investigate the release of Ca^{2+} and OH^- from the ceramsites were carried out by reacting 200 mL of deionized water in 250 mL conical flasks with the ceramsites (2, 4, 6, 8, 10 g). The flasks were immersed in a water bath (Model SHZ-82) at predetermined temperatures (15, 25, 35, 45, 55°C) and then shaken at 150 r/min. The initial pH (2.37, 4.58, 6.45, 8.49, 10.74) was adjusted using 0.1 mol/L NaOH and HCl solutions. Aqueous samples were taken at predetermined intervals (10, 20, 30, 60, 90, 120, 180, 240, 300, 360, 420, 540, 720 min) and then centrifuged at 8000 r/min for 3 min.

Batch experiments for the study of the phosphorus and copper ion removal performance of the ceramsites were carried out by reacting 200 mL of phosphorus (KH_2PO_4) and copper ($CuSO_4$) solutions respectively in 250 mL conical flasks with 4 g of the ceramsites. The flasks were immersed in a

Table 1 – Chemical composition of raw materials (wt.%).

Raw material	SiO_2	Al_2O_3	Fe_2O_3	CaO	MgO	Na_2O	L.O.I[a]	Σ[b]
Lime mud	12.36	0.76	0.34	45.18	2.38	1.47	37.16	99.65
Fly ash	53.54	28.80	6.10	6.82	1.24	1.01	1.86	99.37
Diatomite	88.00	5.36	2.01	0.38	0.64	0.27	2.61	99.27
Kaolin	46.11	37.39	1.23	1.07	0.14	0.07	13.87	99.88

[a] L.O.I: Loss on ignition.
[b] Σ: The summation of SiO_2, Al_2O_3, Fe_2O_3, CaO, MgO, Na_2O and L.O.I contents.

water bath at 25 ± 0.1°C and then shaken at 150 r/min for 720 min. The initial phosphorus concentration was 5 mg/L and the pH was 7.0 ± 0.2. The initial copper ion concentration was 45 mg/L and the pH was 6.25 ± 0.2.

1.3. Analytical methods

The apparent density of the ceramsites was determined according to GB/T 17431.2 (2010). Water absorption and apparent porosity were determined by the Archimedes method (ASTM International, 2000). The cylinder compressive strength of the ceramsites was tested by an electronic universal tester (Model CMT5105). Available lime (CaO) was determined according to BS EN 459–2 (2010). X-ray diffraction (XRD, Model D8 Advance) with CuKα radiation (λ = 0.1542 nm) at 40 kV was used to evaluate the crystalline phases of the ceramsites. Scanning electron microscopy (SEM, Model Quant 250FEG) was performed to observe the pore structure of the ceramsites. Leaching tests were performed using the horizontal vibration method (HJ 557, 2009) and the leach toxicity was tested according to GB 5085.3 (2007) by an inductively coupled plasma mass spectrometer (ICP-MS, Model ICP-MS2000). The horizontal vibration method was undertaken with the solution prepared at a liquid–solid ratio of 10/1 (L/kg) and vibrated at 110 ± 10 r/min for 8 hr, then filtered with a 0.45 μm membrane. Before being analyzed by the ICP-MS, the filtrate was diluted if necessary according to the detection limits of the instrument. The pH values of the aqueous samples were measured by a pH meter (Model PHS-3C) to evaluate the OH^- release of the ceramsites. The Ca^{2+} concentration of the aqueous samples was determined by EDTA titration with a relative error of 0.05% (Kim and Vipulanandan, 2003).

The residual phosphorus concentration was measured using a UV–Visible spectrophotometer (Model EVOLUTION 220) at 700 nm wave length (GB 11893–89, 1990). The residual copper ion concentration was determined by inductively coupled plasma spectrometry (ICP, Model IRIS Intrepid II). The removal rate (R, %) was calculated using the Eq. (1).

$$R = \frac{C_i - C_f}{C_i} \times 100 \quad (1)$$

where C_i (mg/L) and C_f (mg/L) are the initial and final concentrations, respectively.

2. Results and discussion

2.1. Properties of the ceramsites

Table 3 shows the physical and chemical properties of the ceramsites, such as apparent density, 24 hr water absorption, apparent porosity, cylinder compressive strength and available lime content. Through comparison, it can be noticed that 24 hr water absorption and apparent porosity of ceramsites LFS (50wt% lime mud + 45wt% fly ash + 5wt% sawdust) and LFSK (50wt% lime mud + 40wt% fly ash + 5wt% sawdust + 5wt% kaolin) are higher than ceramsites LF (40wt% lime mud + 60wt% fly ash) and LFD (40wt% lime mud + 55wt% fly ash + 5wt% diatomite). Lignin in sawdust was burnt out after sintering at 1050°C for 2 hr, so the addition of sawdust increased the available space in ceramsites for water adsorption. For ceramsites, there is a trend that higher water adsorption and porosity can significantly decrease the density and compressive strength (Zou et al., 2009; Huang et al., 2005). The properties of the ceramsites are in accordance with this trend.

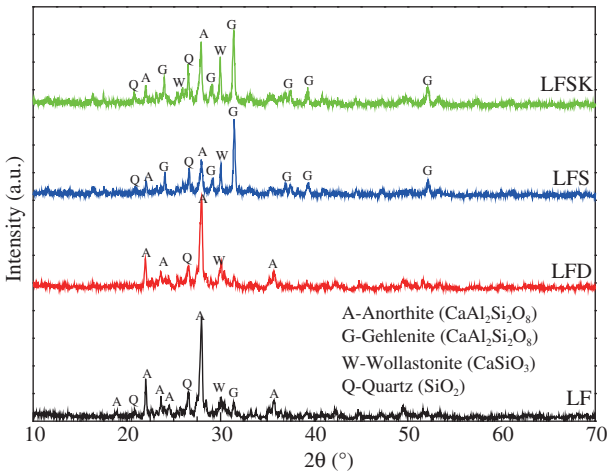

Fig. 1 – XRD patterns of the ceramsites. XRD: X-ray diffraction.

XRD patterns of the ceramsites are shown in Fig. 1. Anorthite ($CaAl_2Si_2O_8$), gehlenite ($Ca_2Al_2SiO_7$), wollastonite ($CaSiO_3$) and quartz (SiO_2) are observed as the main crystalline phases, which were generated from solid state reactions in the sintering process. It has been suggested that low-temperature fabrication (Qin et al., 2015) and the existence of impurities, such as Na and K, reduce the crystal structure stability of anorthite and gehlenite. As a result, in this study part of the anorthite and gehlenite could be dissolved incongruently, as shown in Eqs. (2) and (3) (Shen et al., 1993). In addition, the reaction between available lime and water also brought about more Ca^{2+} and OH^- release, as shown in Eq. (4). Therefore, the existence of these crystalline phases ensured the release of Ca^{2+} and OH^- from the prepared ceramsites.

$$CaAl_2Si_2O_8 + 3H_2O = Ca^{2+} + 2OH^- + Al_2[Si_2O_5][OH]_4 \quad (2)$$

$$2Ca_2Al_2SiO_7 + 9H_2O = 4Ca^{2+} + 6OH^- + 2Al[OH]_4^- + Al_2[Si_2O_5][OH]_4 \quad (3)$$

Table 3 – Physical and chemical properties of the ceramsites.

Sample	Apparent density (g/cm^3)	24 hr water absorption (%)	Apparent porosity (%)	Cylinder compressive strength (MPa)	Available lime (%)
LF	1.368	31.12	43.44	8.62	0.12
LFD	1.218	39.03	49.49	7.80	0.14
LFS	1.039	47.36	53.50	0.79	0.29
LFSK	1.038	47.24	57.39	2.43	0.46

$$CaO + H_2O = Ca^{2+} + 2OH^- \quad (4)$$

Fig. 2 shows the SEM images of the ceramsites. Many connected or open pore scan be observed clearly. These pores were created by the release of accumulated gases, generated from the decomposition of $CaCO_3$ in lime mud and the burning of sawdust. By comparing Fig. 2a–d, it can be seen that ceramsites LFS and LFSK contain more pores than ceramsites LF and LFD, which is in accordance with their water absorption and apparent porosity results.

Lime mud is classified as a toxic industrial waste because of its high alkalinity and the presence of various heavy metal ions. The ceramsites were mainly prepared from waste lime mud and fly ash, so knowledge of the leach toxicity is vital for evaluating the safety of solid waste products. Table 4 presents the leach toxicity results of lime mud and ceramsites LFD and LFSK. Tests were carried out according to the Chinese government standard of Identification standards for hazardous wastes Identification for extraction toxicity (GB 5085.3, 2007). The Cd^{2+} concentration (7.330 mg/L) of the lime mud used in this study is much higher than the limit of the legislation standard (1 mg/L) and its pH is about 13.30, indicating that lime mud is a toxic industrial waste. By contrast, all the tested element concentrations of the leachates of ceramsites LFD and LFSK are lower than the limits of the legislation standard, indicating that the ceramsites prepared from lime mud are green materials and they can be used in the treatment of wastewater.

Table 4 – Leach toxicity of lime mud and ceramsites (mg/L).

Item	Detection limit [a]	Lime mud	LFD	LFSK	Standard [b]
As^{3+}	0.1–1	0.021	0.010	0.012	5
Hg^{2+}	0.1–1	ND [c]	ND	ND	0.1
Ag^{+}	<0.1	ND	ND	ND	5
Se	0.1–1	0.093	0.003	0.001	1
Cr^{3+}	0.1–1	2.150	ND	0.193	15
Cd^{2+}	<0.1	7.330	ND	0.915	1
Cu^{2+}	<0.1	0.006	0.015	0.014	100
Pb^{2+}	<0.1	3.400	0.474	0.591	5
Zn^{2+}	0.1–1	0.108	0.132	0.189	100
Ni^{2+}	0.1–1	0.158	2.195	0.804	5
Be^{2+}	0.1–1	0.200	0.018	0.012	0.02
Ba^{2+}	<0.1	0.018	0.036	0.030	100

[a] Detection Limit ranges of ICP-MS (ppt, 1 ppt = 10^{-6} mg/L).
[b] Limits of standard GB 5085.3, 2007.
[c] ND: below ICP-MS detection limits.

2.2. Factors affecting the release of Ca^{2+} and OH^-

2.2.1. Effect of formulation

Fig. 3 shows the efficiency of Ca^{2+} and OH^- release for different ceramsites. Obviously, ceramsites LFS and LFSK released more Ca^{2+} and OH^- than ceramsites LF and LFD. The release process can be divided into two steps: a rapid initial release (about 0–60 min) mainly due to the rapid reaction in Eq. (4), and a slower subsequent release, mainly due to the slow reactions in Eqs. (2) and (3). Then, the concentrations and pH values became constant, *i.e.*, equilibrium was attained. The Ca^{2+} concentrations released from ceramsites LF, LDS, LFS and LFSK were 40.97, 41.62, 93.34, and 92.20 mg/L, respectively, at 720 min. Accordingly, the release of OH^- kept the pH values of the aqueous solutions in the range of 9.3–9.8 for ceramsites LF and LFD, and 10.0–10.5 for ceramsites LFS and LFSK.

The experimental data for the Ca^{2+} release of different ceramsites was plotted according to the Avrami kinetic model, as shown in Eq. (5) (Demirkiran and Kunkul, 2007),

$$-\ln(1-x) = kt^n \quad (5)$$

where k is the kinetic constant, n is the characteristic constant of the solid, t is the reaction time (min) and x is the fractional

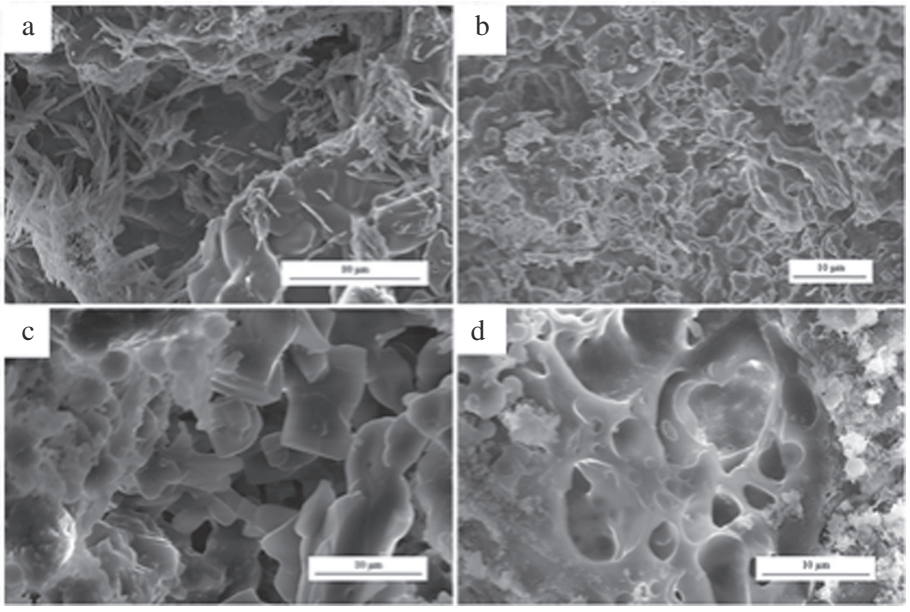

Fig. 2 – SEM images of the ceramsites. (a) LF (40 wt.% lime mud +60 wt.% fly ash); (b) LFD (40 wt.% lime mud +55 wt.% fly ash +5 wt% diatomite); (c) LFS (50 wt.% lime mud +45 wt.% fly ash +5 wt.% sawdust); (d) LFSK (50 wt.% lime mud +40 wt.% fly ash +5 wt.% sawdust +5 wt.% kaolin). SEM: scanning electron microscopy;

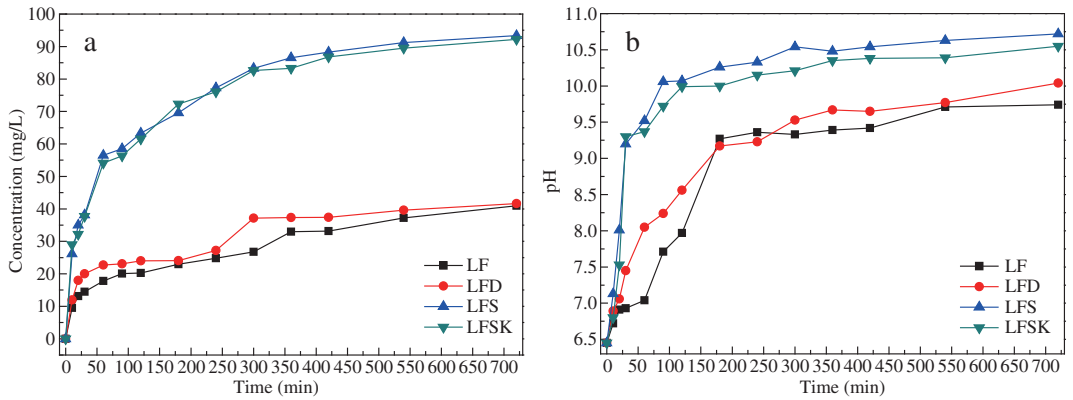

Fig. 3 – Ca^{2+} concentrations (a) and pH values (b) of the aqueous solutions in contact with different ceramsites. Conditions: dosage = 4 g/200 mL, temperature = 25°C, initial pH = 6.45.

conversion. $x = C_t/C_{max}$, and C_t (mg/L) is the concentration at time t while C_{max} is the maximum concentration (mg/L). The characteristic constant n is 0.9019 (Guan et al., 2013). The kinetic constants (k) were determined by fitting the Avrami kinetic model to the experimental data obtained from Fig. 3a. Table 5 presents the results of the fitting. The correlation coefficients (R^2) indicate that this model can describe the Ca^{2+} release of ceramsites LFS and LFSK better than ceramsites LF and LFD. Moreover, the rates of Ca^{2+} release (k) for ceramsites LFS and LFSK were faster than for ceramsites LFS and LFSK, which is in good agreement with Fig. 3a.

Guan et al. (2013) reported that Ca^{2+} was released faster in calcium-rich materials with larger specific surface areas. In Table 3 and Fig. 2, the apparent porosities of ceramsites LFS and LFSK are significantly higher than those of ceramsites LF and LFD, indicating that ceramsites LFS and LFSK have better pore structure and larger specific surface area. Therefore, the efficiencies of Ca^{2+} and OH^- release for ceramsites LFS and LFSK were higher than for ceramsites LF and LFD. In consideration of the cylinder compressive strength (0.79 and 2.43 MPa for ceramsites LFS and LFSK, respectively), ceramsite LFSK was selected as the best candidate to investigate the other factors.

The mechanism of Ca^{2+} and OH^- release was further investigated by XRD. In Fig. 1, anorthite was identified as the major phase of ceramsites LF and LFD, while gehlenite was the major phase of ceramsites LFS and LFSK. The results in Fig. 3 can infer that the capacity for Ca^{2+} and OH^- release from gehlenite is stronger than that of anorthite. In addition, the XRD patterns of ceramsite LFSK before and after the batch experiments are compared in Fig. 4. It can be seen that the release of Ca^{2+} and OH^- did not affect the main crystalline phases markedly, with a diffuse peak appearing in the range of 2θ = 10–20°. During the batch experiments, part of the anorthite and gehlenite in the ceramsites were dissolved to release Ca^{2+} and OH^-, which resulted in grain refinement and even the development of an amorphous phase. These changes in crystal structures were reflected in the XRD patterns by the appearance of a diffuse peak in the range 2θ = 10–20° (Ma, 2004; Li, 1988).

Table 5 – Correlation equations and rate constants for the Avrami kinetic model describing Ca^{2+} release.

Sample no.	Correlation equation	k	R^2
LF	$-\ln(1-x) - 0.0077t^{0.9019}$	0.0077	0.9135
LFD	$-\ln(1-x) - 0.0106t^{0.9019}$	0.0106	0.8949
LFS	$-\ln(1-x) - 0.0130t^{0.9019}$	0.0130	0.9708
LFSK	$-\ln(1-x) - 0.0125t^{0.9019}$	0.0125	0.9614

2.2.2. *Effect of dosage*

Fig. 5 shows the efficiency of Ca^{2+} and OH^- release for ceramsite LFSK as a function of dosage between 2 and 10 g. The Ca^{2+} concentrations were 58.99, 92.20, 138.48, 147.45, and 156.47 mg/L for dosages of 2, 4, 6, 8, and 10 g, respectively at 720 min. Accordingly, the release of OH^- maintained the pH values in the range of 10.2–10.9. The differences in the Ca^{2+} and OH^- release were mainly reflected in the slower subsequent release process, and Ca^{2+} concentrations were not always increased in direct proportion to the dosage. Therefore, these results can provide a reference for the selection of dosage in wastewater treatment.

2.2.3. *Effect of temperature*

Fig. 6 shows the efficiency of Ca^{2+} and OH^- release for ceramsite LFSK when the temperatures of batch experiments

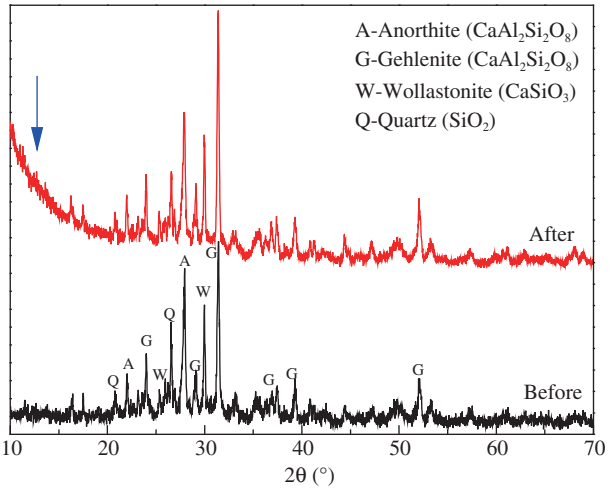

Fig. 4 – XRD patterns of ceramsite LFSK before and after the batch experiments. Conditions: dosage = 4 g/200 mL, temperature = 25°C, initial pH = 6.45.

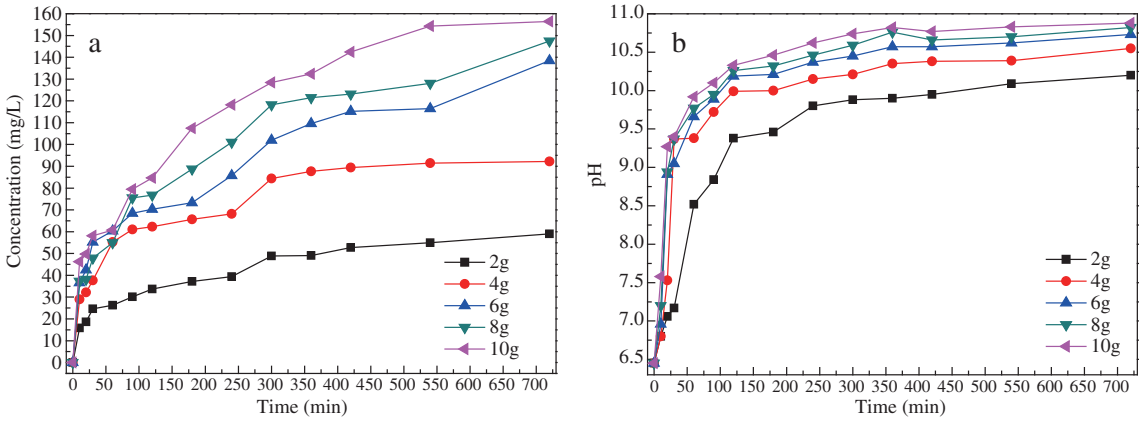

Fig. 5 – Ca^{2+} concentrations (a) and pH values (b) of the aqueous solutions with different dosages. Conditions: ceramsite LFSK, temperature = 25°C, initial pH = 6.45.

were changed between 15 and 55°C. Ca^{2+} concentrations were in the range of 84.86–123.37 mg/L at 720 min, increasing with the increased temperature. Above 35°C, the slower subsequent release process was extended because high temperature could promote the dissolution of anorthite and gehlenite. However, the release of OH^- still kept the pH values within 10.3–10.9 and no dramatic changes occurred with the increase of temperature. Therefore, the prepared ceramsites

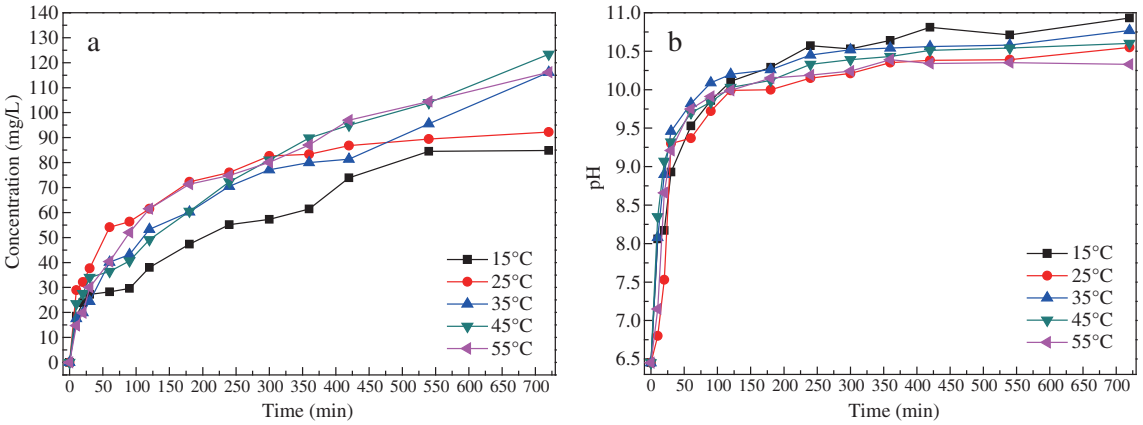

Fig. 6 – Ca^{2+} concentrations (a) and pH values (b) of the aqueous solutions at different temperatures. Conditions: ceramsite LFSK, dosage =4 g/200 mL, initial pH = 6.45.

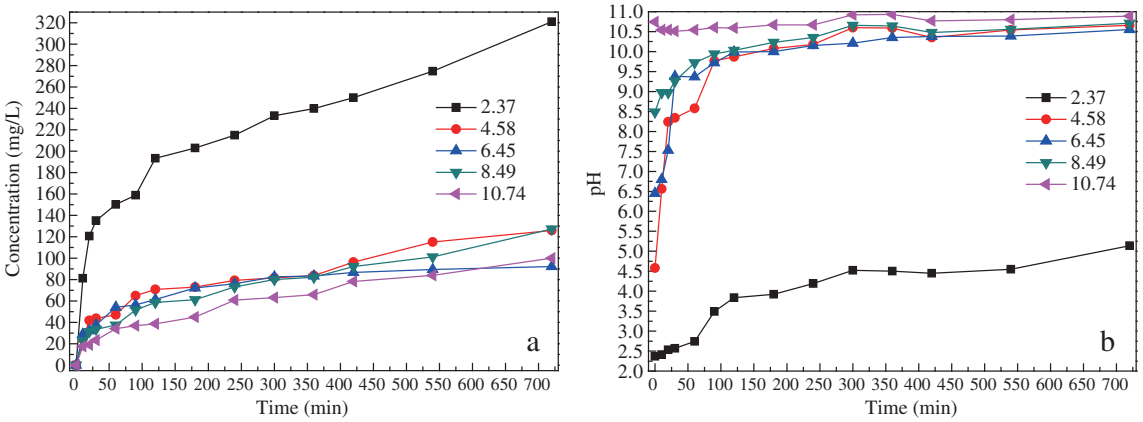

Fig. 7 – Ca^{2+} concentrations (a) and pH values (b) of the aqueous solutions with different initial pH. Conditions: ceramsite LFSK, dosage =4 g/200 mL, temperature = 25°C.

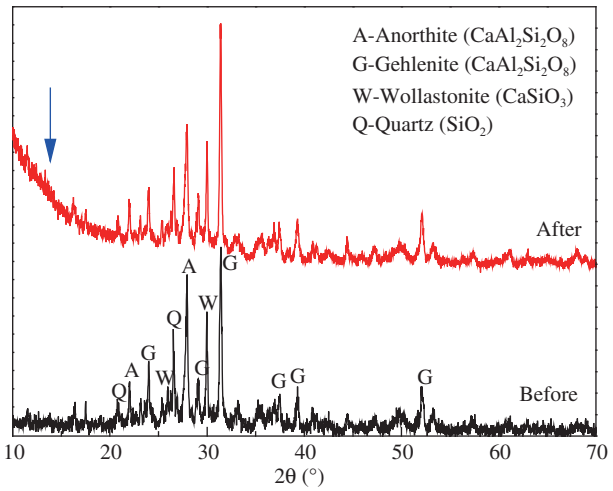

Fig. 8 – XRD patterns of ceramsite LFSK before and after the batch experiments. Conditions: dosage = 4 g/200 mL, temperature = 25°C, initial pH = 2.37.

can be used in wastewater under various temperature conditions.

2.2.4. Effect of initial pH

Fig. 7 shows the change in the efficiency of Ca^{2+} and OH^- release for ceramsite LFSK when the initial pH values of the aqueous solutions were changed between 2.37 and 10.74. As can be observed, the Ca^{2+} concentrations and OH^- values displayed no obvious differences except when the initial pH was 2.37. As the initial pH changed from 4.68 to 10.74, Ca^{2+} concentrations were in the range of 92.20–127.39 mg/L and the final pH values were in the range of 10.6–10.9 at 720 min. However, Ca^{2+} concentrations showed a sharp increase to 321.08 mg/L and the final pH value was decreased to 5.14 at 720 min when the initial pH value was 2.37. Moreover, after 720 min the slower release process for the ceramsite was still taking place. It is known that wollastonite is not stable in hydrochloric acid, so a portion of this phase in the ceramsite might be dissolved, as shown in Eq. (6), causing the increase in Ca^{2+} concentration. In addition, most of the OH^- released from the ceramsite was reacted with H^+ to increase the pH of the aqueous solution, as shown in Eq. (7). It can be suggested that the prepared ceramsites have the ability to adjust the pH of wastewater. Notably, they can keep both weak acidic and alkaline wastewaters in an alkaline condition finally and have no obvious influence on the release of Ca^{2+}.

$$CaSiO_3 + 2H^+ = Ca^{2+} + SiO_2 + H_2O \quad (6)$$

$$H^+ + OH^- = H_2O \quad (7)$$

In order to investigate the further influence of acidic aqueous solution (pH = 2.37) on the ceramsite, XRD patterns of ceramsite LFSK before and after the batch experiments are shown in Fig. 8. It can be seen that acidic aqueous solution did not affect the main crystalline phases notably and a diffuse peak in the range of 2θ = 10–20° is also observed, indicating that microscopic changes in the crystal structures took place. Therefore, the prepared ceramsites can be used in wastewater under various pH conditions.

2.3. Application performance of the ceramsites

In order to evaluate the capability of the prepared ceramsites in wastewater treatment, the phosphorus and copper ion removal performance was investigated. Fig. 9 shows the removal rates and the final pH values for the treatment. Clearly, ceramsites LFS and LFSK are very much superior to ceramsites LF and LFD in the removal of ions and the adjustment of pH values. The removal rates of phosphorus and copper ions by ceramsite LFSK were 96.88% and 94.84%, respectively, as shown in Fig. 9a. The final pH values of phosphorus solutions showed almost no change, and the final pH values of copper ion solutions with ceramsites LF, LFD and LFS were all decreased; however, the pH of the solution in contact with ceramsite LFSK still remained at about 10.6. According to the distribution diagram for phosphate as a function of pH (Clifford, 1961), phosphate existed in the form of HPO_4^{2-} in the pH range 9.6–9.9, and in the forms of HPO_4^{2-} and PO_4^{3-} in the pH range 10.0–10.8. Therefore, the phosphorus removal performance of the ceramsites can be described through Eqs. (8) and (9). The copper ion removal of the

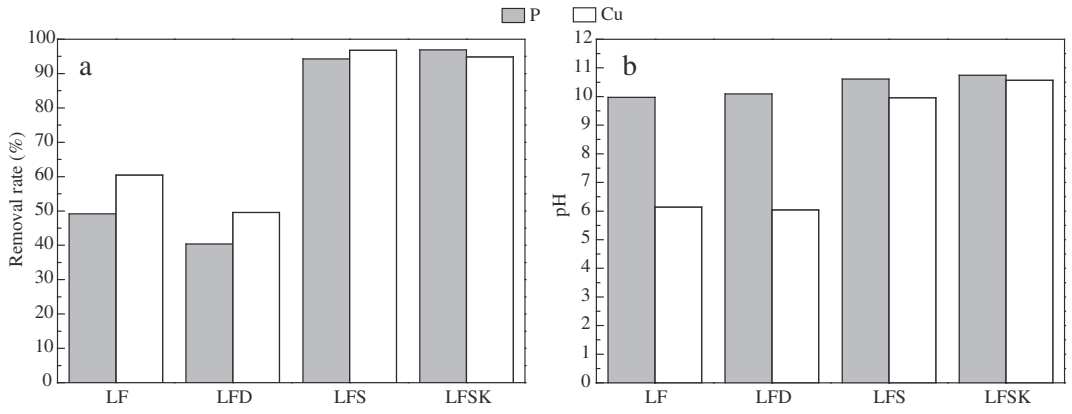

Fig. 9 – Removal rates (a) and final pH values (b) for phosphorus and copper ion removal by the ceramsites.

ceramsites involves the consumption of OH^-, as shown in Eq. (10).

$$Ca^{2+} + HPO_4^{2-} = CaHPO_4\downarrow \quad (8)$$

$$3Ca^{2+} + 2PO_4^{3-} = Ca_3(PO_4)_2\downarrow \quad (9)$$

$$Cu^{2+} + 2OH^- = Cu(OH)_2\downarrow \quad (10)$$

3. Conclusions

Lime mud and fly ash were successfully recycled in the production of ceramsites through solid state reactions at 1050°C. The properties, crystalline phases and microstructure of the prepared ceramsites were characterized. The effects of formulation, dosage, temperature, initial pH and contact time on the release of Ca^{2+} and OH^- from the ceramsites were investigated on the basis of batch experiments. The phosphorus and copper ion removal performance of the ceramsites was also evaluated.

The following specific conclusions have been deduced from this study.

(1) Ca^{2+} and OH^- were released from the ceramsites mainly due to the dissolution of anorthite, gehlenite and available lime. Compared with anorthite, gehlenite had a stronger capacity for Ca^{2+} and OH^- release.
(2) The Ca^{2+} release was well-fitted by the Avrami kinetic model. Increases in porosity, dosage and temperature were associated with increases in Ca^{2+} concentration.
(3) The ceramsites had a strong ability to change the pH of aqueous solutions. Notably, under various conditions they could still maintain aqueous solutions in alkaline conditions (pH = 9.3–10.9) and the release of Ca^{2+} was not affected.
(4) The release of Ca^{2+} and OH^- was the key to phosphorus and copper ion removal. The removal rates of phosphorus and copper ions were as high as 96.88% and 96.81%, respectively.

Acknowledgments

This work was financially supported by the National Natural Science Foundation of China (Nos. 51578289 and 51468053), the Technology Major Projects of China (No. 2012ZX04010-032), the Research and innovation program of graduate students in Jiangsu Province (No. KYLX_0347) and the Innovation Fund for National Small and Medium Technology Based Firms of China (No. 11C26213201410).

REFERENCES

Ahmadi, B., Al-Khaja, W., 2001. Utilization of paper waste sludge in the building construction industry. Resour. Conserv. Recycl. 32 (2), 105–113.

ASTM International, 2000. Standard test methods for apparent porosity, water absorption, apparent specific gravity and bulk density of burned refractory brick shapes by boiling water, C-20. Annual book of ASTM standards.

Battistoni, P., Pavan, P., Cecchi, F., Mata-Alvarez, J., 1998. Phosphate removal in real anaerobic supernatants: Modelling and performance of a fluidized bed reactor. Water Sci. Technol. 38 (1), 275–283.

BE EN 196–2, 2013. Methods of testing cement—Part 2: Chemical analysis of cement. Brussels.

BS EN 459–2, 2010. Building lime—Part 2: Test methods. Brussels.

Cernec, F., Zule, J., Moze, A., Ivanu, A., 2005. Chemical and microbiological stability of waste sludge from paper industry intended for brick production. Waste Manag. Res. 23 (2), 106–112.

Cheng, J., Zhou, J., Liu, J., Cao, X., Cen, K., 2009. Physicochemical characterizations and desulfurization properties in coal combustion of three calcium and sodium industrial wastes. Energy Fuel 23 (-), 2506–2516.

Clifford, A.F., 1961. Inorganic chemistry of quantitative analysis. Prentice Hall, New Jersey.

Demirkiran, N., Kunkul, A., 2007. Dissolution kinetics of ulexite in perchloric acid solutions. Int. J. Miner. Process. 83 (s 1–2), 76–80.

Fujimoto, N., Mizuochi, T., Togami, Y., 1991. Phosphorus fixation in the sludge treatment system of a biological phosphorus removal process. Water Sci. Technol. 23, 635–640.

GB 11893–89, 1990. Water quality—Determination of total phosphorus—Ammonium molybdate spectrophotometric method. Beijing.

GB 5085.3, 2007. Identification standards for hazardous wastes—Identification for extraction toxicity. Beijing.

GB/T 17431.2, 2010. Lightweight aggregates and its test methods. Part 2: Test methods for lightweight aggregates. Beijing.

Guan, W., Ji, F.Y., Chen, Q.K., Yan, P., Zhang, Q., 2013. Preparation and phosphorus recovery performance of porous calcium-silicate-hydrate. Ceram. Int. 39 (2), 1385–1391.

HJ 557, 2009. Solid waste—Extraction procedure for leaching toxicity—Horizontal vibration method. Beijing.

Huang, C.P., Pan, J.R.S., Liu, Y.R., 2005. Mixing water treatment residual with excavation waste soil in brick and artificial aggregate making. J. Environ. Eng. 131 (2), 272–277.

Huber, P., Ossard, S., Fabry, B., Bermond, C., Craperi, D., Fourest, E., 2014. Conditions for cost-efficient reuse of biological sludge for paper and board manufacturing. J. Clean. Prod. 66 (2), 65–74.

Kaasik, A., Vohla, C., Mõtlp, R., Mander, Ü., Kirsimä, K., 2008. Hydrated calcareous oilshale ash as potential filter media for phosphorus removal in constructed wetlands. Water Res. 42 (s 4–5), 1315–1323.

Kim, J., Vipulanandan, C., 2003. Effect of pH, sulfate and sodium on the EDTA titration of calcium. Cem. Concr. Res. 33 (5), 621–627.

Li, S.T., 1988. X-ray diffraction of crystals. Central South University, Hunan (In Chinese).

Li, N., Zhang, L., Chen, Y., Tian, Y., Wang, H., 2011. Adsorption behavior of Cu(II) onto titanate nanofibers prepared by alkali treatment. J. Hazard. Mater. 189 (1–2), 265–272.

Liira, M., Kõiv, M., Mander, Ü., Mõtlep, R., Vohla, C., Kirsimäe, K., 2009. Active filtration of phosphorus on Ca-rich hydrated oil shale ash: does longer retention time improve the process? Environ. Sci. Technol. 43 (10), 3809–3814.

Liu, Y.J., Naidu, R., Ming, H., 2011. Red mud as an amendment for pollutants in solid and liquid phases. Geoderma 163, 1–12.

Liu, J.B., Ye, X.Y., Wang, H., Zhu, M.K., Wang, B., Yan, H., 2003. The influence of pH and temperature on the morphology of hydroxyapatite synthesized by hydrothermal method. Ceram. Int. 29 (6), 629–633.

Ma, L.D., 2004. The diffraction of polycrystal by X ray in the modern — The experimental technology and data analysis. Chemical Industry Press, Beijing (In Chinese).

Martins, F.M., Martins, J.M., Ferracin, L.C., da Cunha, C.J., 2007. Mineral phases of green liquor dregs, slaker grits, lime mud

and wood ash of a Kraft pulp and paper mill. J. Hazard. Mater. 147 (s 1–2), 610–617.
Monte, M.C., Fuente, E., Blanco, A., Negro, C., 2009. Waste management from pulp and paper production in the European Union. Waste Manag. 29 (1), 293–308.
Qin, J., Cui, C., Cui, X.Y., Ahmad, H., Yang, C.M., Yang, S.H., 2015. Recycling of lime mud and fly ash for fabrication of anorthite ceramic at low sintering temperature. Ceram. Int. 41 (4), 5648–5655.
Shen, Z.L., Zhu, W.H., Zhong, Z.S., 1993. The foundation of hydrogeochemistry. Geological Publishing House, Beijing (In Chinese).
Song, Y., Weidler, P.G., Berg, U., Nüesch, R., Donnert, D., 2006. Calcite-seeded crystallization of calcium phosphate for phosphorus recovery. Chemosphere 63 (2), 236–243.
Stafiej, A., Pyrzynska, K., 2008. Adsorption of heavy metal ions with carbon nanotubes. Sep. Purif. Technol. 58 (1), 49–52.
Sthiannopkao, S., Sreesai, S., 2009. Utilization of pulp and paper industrial wastes to remove heavy metals from metal finishing wastewater. J. Environ. Manag. 90 (11), 3283–3289.
Sun, R.Y., Li, Y.J., Liu, C.T., Xie, X., Lu, C.M., 2013. Utilization of lime mud from paper mill as CO_2 absorbent in calcium looping process. Chem. Eng. J. 221 (4), 124–132.
Tofighy, M.A., Mohammadi, T., 2011. Adsorption of divalent heavy metal ions from water using carbon nanotube sheets. J. Hazard. Mater. 185 (1), 140–147.
Vohla, C., Koiv, M., Bavor, H.J., Chazarenc, F., Mander, U., 2011. Filter materials for phosphorus removal from wastewater in treatment wetlands: A review. Ecol. Eng. 37 (1), 70–89.
Wirojanagud, W., Tantemsapya, N., Tantriratna, P., 2004. Precipitation of heavy metals by lime mud waste of pulp and paper mill. Songklanakarin J. Sci. Technol. 26, 45–53 (Suppl.).
Xu, G.R., Zou, J.L., Dai, Y., 2006. Utilization of dried sludge for making ceramsite. Water Sci. Technol. 54 (9), 69–79.
Xu, G.R., Zou, J.L., Li, G.B., 2008. Effect of sintering temperature on the characteristics of sludge ceramsite. J. Hazard. Mater. 150 (2), 394–400.
Yan, H., Yang, L., Yang, Z., Yang, H., Li, A., Cheng, R., 2012. Preparation of chitosan/poly (acrylic acid) magnetic composite microspheres and applications in the removal of copper(II) ions from aqueous solutions. J. Hazard. Mater. 229-230, 371–380.
Yin, H.B., Yun, Y., Zhang, Y.L., Fan, C.X., 2011. Phosphate removal from wastewaters by a naturally occurring, calcium-rich sepiolite. J. Hazard. Mater. 198 (2), 362–369.
Zhang, J., Wang, Q., Jiang, J., 2013. Lime mud from paper-making process addition to food waste synergistically enhances hydrogen fermentation performance. Int. J. Hydrog. Energy 38 (6), 2738–2745.
Zou, J.L., Xu, G.R., Li, G.B., 2009. Ceramsite obtained from water and wastewater sludge and its characteristics affected by Fe_2O_3, CaO, and MgO. J. Hazard. Mater. 165 (s 1–3), 995–1001.